Physics and Imaging in Radiation Oncology 29 (2024) 100549

Contents lists available at ScienceDirect

Physics and Imaging in Radiation Oncology

journal homepage: www.sciencedirect.com/journal/physics-and-imaging-in-radiation-oncology

Original Research Article

Script-based implementation of automatic grid placement for lattice stereotactic body radiation therapy

Wesley W. Tucker [a,*,1], Thomas R. Mazur [a,1], Matthew C. Schmidt [a], Jessica Hilliard [a], Shahed Badiyan [a], Matthew B. Spraker [b], James A. Kavanaugh [c]

[a] Department of Radiation Oncology, Washington University in St. Louis, St. Louis, MO 63110 USA
[b] Department of Radiation Oncology, Centura Health, Denver, CO 80210 USA
[c] Department of Radiation Oncology, Mayo Clinic, Rochester, MN 55905 USA

ARTICLE INFO

Keywords:
Spatial fractionation
Lattice SBRT
Plan automation

ABSTRACT

Background and purpose: Spatially fractionated radiation therapy (SFRT) has demonstrated promising clinical response in treating large tumors with heterogeneous dose distributions. Lattice stereotactic body radiation therapy (SBRT) is an SFRT technique that leverages inverse optimization to precisely localize regions of high and lose dose within disease. The aim of this study was to evaluate an automated heuristic approach to sphere placement in lattice SBRT treatment planning.

Materials and methods: A script-based algorithm for sphere placement in lattice SBRT based on rules described by protocol was implemented within a treatment planning system. The script was applied to 22 treated cases and sphere distributions were compared with manually placed spheres in terms of number of spheres, number of protocol violations, and time required to place spheres. All cases were re-planned using script-generated spheres and plan quality was compared with clinical plans.

Results: The mean number of spheres placed excluding those that violate rules was greater using the script (13.8) than that obtained by either dosimetrist (10.8 and 12.0, $p < 0.001$ and $p = 0.003$) or physicist (12.7, $p = 0.061$). The mean time required to generate spheres was significantly less using the script (2.5 min) compared to manual placement by dosimetrists (25.0 and 29.9 min) and physicist (19.3 min). Plan quality indices were similar in all cases with no significant differences, and OAR constraints remained met on all plans except two.

Conclusion: A script placed spheres for lattice SBRT according to institutional protocol rules. The script-produced placement was superior to that of manually-specified spheres, as characterized by sphere number and rule violations.

1. Introduction

For hypofractionated treatment of large tumor volumes, spatially fractioned radiotherapy (SFRT) has been demonstrated to be a compelling alternative scheme for radiation delivery [1–3]. SFRT has been practiced for nearly a century, with underlying hypotheses supporting its application including 1) stimulating immune response and bystander effects and 2) sparing healthy tissues [4–8]. While stereotactic body radiation therapy (SBRT) is often an effective treatment for patients with metastatic or unresectable tumors, it has been shown – specifically in non-small cell lung cancer – to lead to higher toxicity in tumors greater than 100 cm^3 volume or 5.7 cm diameter compared with smaller tumors [9]. Historically SFRT has been achieved with static collimators and grid-like apertures, and tumors have been treated with simplistic geometries including one or two angles of incidence [10–13]. With modern techniques, additional degrees-of-freedom enable customization and streamlined placement of peaks and valleys in dose distributions [14–19].

Recently, a five fraction form of volumetric modulated arc therapy (VMAT) -based SFRT, known as lattice SBRT, was developed. With lattice SBRT, custom patterns of high-dose peaks and low-dose valleys are produced by placement of associated high-dose spheres (HDS) and low-dose spheres (LDS) in a grid-like pattern within the tumor. Initial studies suggest favorable response for large tumors without toxicity to adjacent

* Corresponding author.
E-mail address: tuckerw@wustl.edu (W.W. Tucker).
[1] W.W.T. and T.R.M. contributed equally to this manuscript and share first authorship.

https://doi.org/10.1016/j.phro.2024.100549
Received 15 September 2023; Received in revised form 26 January 2024; Accepted 5 February 2024
Available online 9 February 2024

organs at risk (OAR) [20]. On institutional Phase I and Phase II protocols, almost 100 patients were treated with this technique between 2019 and 2022 [21]. Other approaches have been developed for inversely-planned SFRT. For example, Grams et al. described a similar approach that places 1.5 cm diameter HDS at least 3 cm apart within a gross tumor volume (GTV) and at least 1 cm from any OAR [14]. Wu et al. described a similar VMAT-based approach but with variable sphere diameter and separation and also dose to vertices and GTV [15]. Borzov et al. likewise used VMAT planning to demonstrate feasibility of treating high-dose cylinders in single fraction amidst a course of conventional fractionation for three soft tissue sarcoma cases [22]. While these approaches among others are similar, differences in rules and approaches for high dose placement introduce variations in treatment planning dose and volume endpoints between sites that preclude meaningful comparisons of response and outcome [2,18,19,23,24].

As these techniques expand in application, promoting standardized practice in terms of prescribing and achieving spatial fractionation is important for assessing response and outcome. An advantage of a previously described rule-based lattice SBRT approach is that spheres are placed on a well-defined grid such that vertex-to-vertex spacing and dose gradients are standardized [17]. While this approach is rule-based, identifying appropriate vertex placement within the tumor volume according to rules can be time-consuming, especially for targets with unusual shape and aspect ratio. While the manual sphere placement follows set guidelines, the pattern ultimately prepared can be subjective and prone to deviations from rules in an effort to add spheres according to prior experience, which in turn could result in variable dosimetry in terms of lattice-specific planning indices such as peak-to-valley dose ratio. Because this is a rule-based approach, sphere placement can in principle be automated to reduce treatment planning time and ensure that spheres are consistently placed to minimize variation in the achieved spatial fractionation.

In this study, we aim to develop an automated, rule-based technique for sphere placement to support standardized treatment planning and evaluation in lattice SBRT. We specifically outline an algorithm that aims to maximize sphere number in a GTV according to previously outlined rules. We describe a script-based implementation of this algorithm, and retrospectively apply this script to previously treated lattice SBRT cases to compare user-placed and script-created sphere arrangements in terms of geometry and efficiency. We then re-plan these cases with script-generated spheres to compare plan dosimetry in terms of lattice-specific and conventional plan metrics.

2. Materials and methods

Treatment plan information was collected for 21 patients (22 plans) consecutively treated via lattice SBRT at our institution from 2020 to 2021. All data was collected with approval by an institutional review board with waiver of informed consent. Patients were treated in 5 fractions, with 20 Gy delivered to PTV_2000 defined as gross tumor volume (GTV) plus setup margin (5 – 8 mm in most cases) and 66.7 Gy delivered as a simultaneous integrated boost to lattice spheres prepared as PTV_6670. PTV_6670 sphere arrangements were manually defined by dosimetrists and physicists according to rules specified in an institutional protocol. The grid pattern defined in the protocol was created in an effort to achieve a dose gradient between 66.7 Gy and 20 Gy within 1.5 cm.

2.1. Sphere placement rules

As shown schematically in Fig. 1, these HDS within PTV_6670 were 1.5 cm in diameter and placed on axial planes of the CT acquisition used for treatment planning. On each plane, the lattice consisted of alternating HDS and LDS spaced 3 cm apart center-to-center in both in-plane directions. Planes were spaced by 3 cm between layers in the superior-inferior directions. Within a given axial plane, HDS were placed on diagonal elements of the grid, and were only placed on vertices where the entire sphere was confined within the GTV retracted by 5 – 15 mm per discretionary judgement based on GTV proximity to OARs. On adjacent axial planes, HDS were offset by 3 cm along the grid axes. The grid

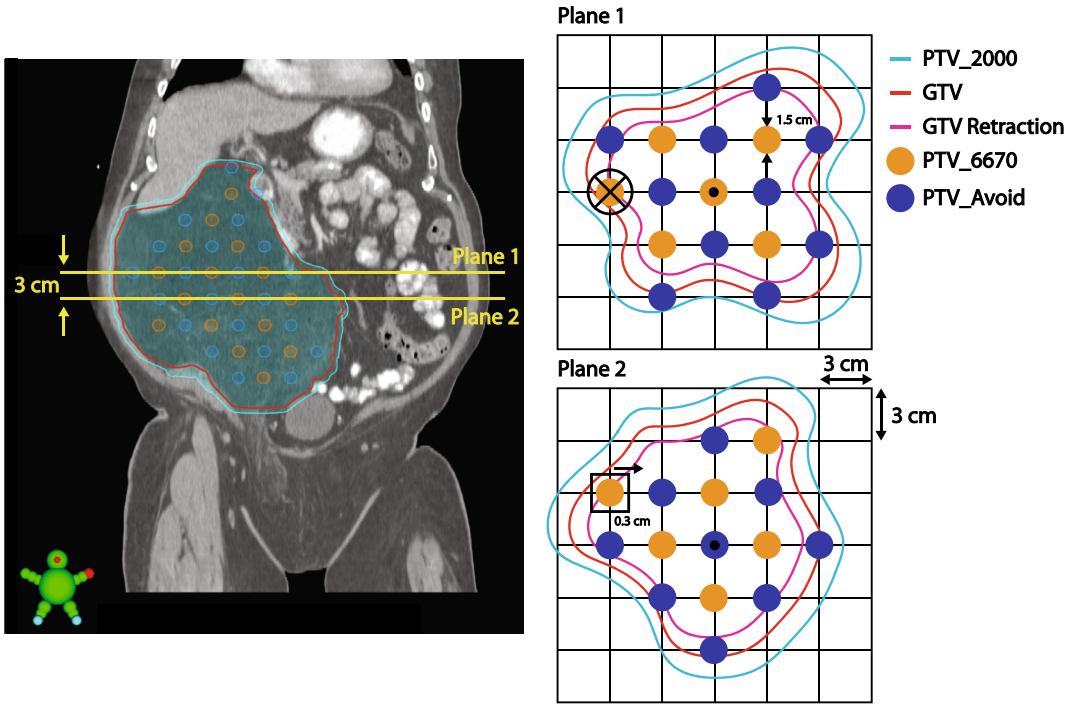

Fig. 1. Schematic of sphere arrangement in PTV_6670 (orange) and PTV_Avoid (blue). Spheres are 1.5 cm in diameter and arranged on vertices of a square 3 cm grid oriented on axial slices of the CT acquisition. HDS spheres must be placed diagonal to each other and be confined within a GTV retraction (magenta). LDS are placed on vertices adjacent to the HDS and must be confined within PTV_2000 (cyan). (For interpretation of the references to colour in this figure legend, the reader is referred to the web version of this article.)

placement relative to the GTV was typically iteratively adjusted via 3D translation in an effort to maximize the number of HDS that populate the GTV retraction. Additionally, the grid could be rotated about the transverse axis, but rotations around other axes were disallowed.

Because in clinical practice spheres were manually placed, we provided flexibility in exact sphere placement. For example, individual spheres could be offset by up to 3 mm from the intended vertex. Likewise, given that many GTVs had unique shapes and aspect ratios, on superior- and inferior-most planes with a single sphere, HDS were allowed to automatically be positioned at the target centroid on that slice. LDS were arranged in the same pattern, but translated by 3 cm from the HDS. The LDS – contoured within structure labeled PTV_Avoid – could extend beyond GTV, but needed to be confined to the PTV_2000 because a minimum dose coverage objective was included in optimization for this structure.

2.2. Script design

The rules outlined above and depicted in Fig. 1 were translated to a C#-based script implemented within the treatment planning system using a vendor-provided application program interface (Eclipse Scripting API or ESAPI, Eclipse V15.6, Varian Medical Systems). The algorithm initially created structures *S1* and *S2*. *S1* was a retraction of the GTV created by applying an isotropic, negative margin to the GTV. This structure was the boundary in which all HDS must ultimately be contained, and its margin was user configurable. *S2* was another GTV retraction with an inner margin 3 mm less than that applied to *S1*. *S2* was the boundary for sphere placement by the algorithm given that spheres may be displaced 3 mm from their vertices. The algorithm also created a bounding box, labeled *S3*, as the maximum grid extent in searching for optimum sphere placement. Dimensions of *S3* corresponded to maximum PTV extent along cardinal patient axes, plus added margin to accommodate two vertex positions on each side of the bounding box. Fig. 2 outlines relevant contours used by the algorithm including *S1*, *S2* and *S3*.

Once structures were initialized, the algorithm then populated all eligible vertices of the lattice grid within *S3* with HDS. Lattice positions were sampled through combinations of angular and translational displacements. Specifically, the lattice was rotated about the cranial-caudal axis in 10 degree increments by up to 90 degrees (given the rotational symmetry of the grid). The lattice was also translated along cardinal axes, including 1) left–right and anterior-posterior in 3 mm increments across 3 cm and superior-inferior in 2 mm increments across 3 cm (with the latter resolution determined by slice thickness of the CT protocols used for patient simulation). Each iteration of angular and translational displacement returned a number of spheres contained within *S2*, and the orientation that yielded the highest number of spheres was selected. An auxiliary structure *S4* was used to evaluate whether a sphere was confined within the GTV retraction through evaluation of its centroid position.

Once the optimal lattice arrangement was determined, PTV_Avoid was populated by LDS on the complementary vertex positions for which the LDS were confined within PTV_2000. Any HDS within *S2* but not in *S1* was translated by up to 3 mm in the direction of the GTV centroid on that slice such that the sphere was ultimately within *S1*. HDS superior or inferior to *S1* but within *S2* were translated inferiorly or superiorly by up to 3 mm to be confined within *S1*. For the superior- and inferior-most grid planes containing HDS, if only a single sphere was present that sphere was translated to the centroid of that slice, and associated LDS on these slices was translated by the same amount.

2.3. Script application and assessment

The script was applied to the 22 cases selected for this study. Sites treated included head-and-neck (1), thorax (6), abdomen (8), pelvis (4) and extremities (3). For the 22 plans considered, median (inter-quartile range, IQR) GTV volume was 1151 cm^3 (1181 cm^3). The time required for the script to execute was recorded for each case and compared to the time needed by two dosimetrists and a medical physicist who actively participate in clinical lattice SBRT treatment planning to manually place spheres. In addition to comparing times, the numbers of spheres placed by the script and each user were recorded, and the number of position violations relative to the rules defined above were tallied. Specifically, violations were recorded for instances 1) where HDS extended outside the specified GTV retraction, 2) when a HDS was moved more than 3 mm in any direction to fit inside GTV as identified by manual review and measurement of each sphere by a physicist, or 3) when LDS extended outside of PTV_2000. Significance was evaluated using a paired *t*-test.

Given that the script cannot incorporate discretionary judgement that might be applied in manual sphere placement, all cases were re-planned using the script-generated spheres and plan quality was compared with the clinical plans. Several conventional plan quality indices were compared between plans, including PTV_6670 V66.7 Gy (%) and conformity index (volume of 66.7 Gy isodose line divided by PTV_6670 vol), PTV_2000 V20Gy (%) and conformity index (volume of 20 Gy isodose line divided by PTV_2000 vol), and monitor unit ratio (plan monitor units divided by daily prescription dose in cGy, i.e. 1334 cGy). Additionally, a sphere *dose ratio* was compared between plans as a

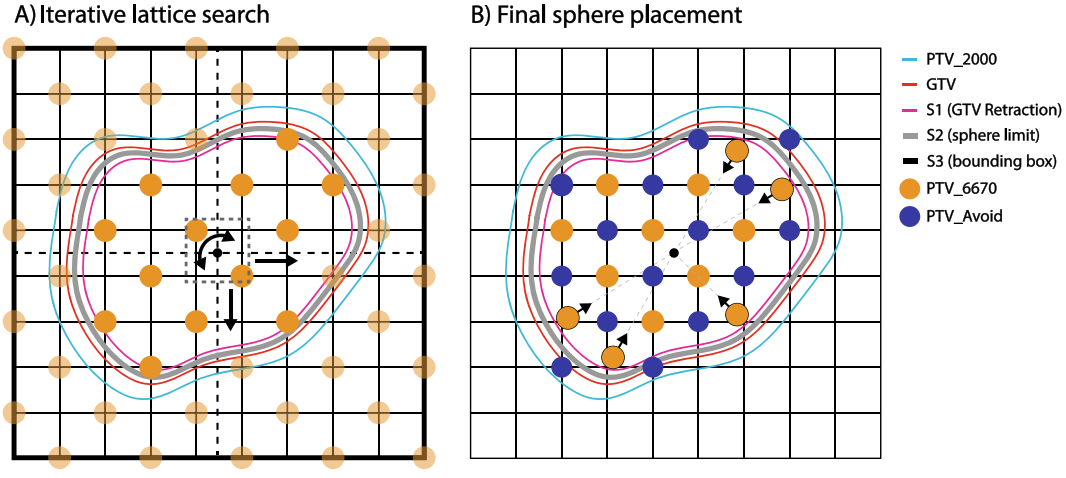

Fig. 2. A) Outline of the construction of the defined space for searching for the optimal lattice orientation and position. HDS are populated on a grid with two vertices buffering each GTV boundary. Lattice positions and orientations are sampled, and for each configuration the number of HDS within *S2* are tallied. B) For the lattice that yields the most spheres within *S2*, sphere positions are fine-tuned to ensure HDS are confined within the user-specified GTV retraction (*S1*).

surrogate for peak-to-valley dose ratio, defined as ratio of mean doses between PTV_6670 and PTV_Avoid. For all cases, re-planning used identical beam geometry to clinical plans, and prioritized institutional OAR constraints which are derived from literature [25,26]. All treatment planning was performed via VMAT within the same TPS used for script-based sphere creation (Eclipse V15.6, Varian Medical Systems). All cases were planned based on an optimization template that aimed to produce PTV_6670 V66.7 Gy > 95 %, PTV_2000 V20Gy > 95 %, monitor unit ratio < 5 and dose ratio > 3. In any instances where sphere position precluded meeting an OAR constraint, the sphere distribution was manually updated.

3. Results

The script created unique sphere distributions for all cases relative to manually-placed distributions, as exemplified in Fig. 3 for two representative cases with GTV volume exceeding 1000 cm^3.

As summarized in Fig. 4, average sphere number for script-based plans was 13.8, with zero sphere position violations by virtue of the rule-based placement. In contrast, mean sphere numbers (violation numbers) were 12.5 (1.7) for dosimetrist one, 13.6 (1.6) for dosimetrist two, and 15.6 (2.9) for the medical physicist. Differences in the number of spheres excluding sphere violations were statistically significant between script-based and all manually-placed plans (see tabular data in supplementary material). Using the script, the mean time for sphere placement was 2.5 ± 1.7 min, compared to 29.9 ± 12.9 min ($p < 0.001$) for dosimetrist one, 25.0 ± 10.7 min ($p < 0.001$) for dosimetrist two, and 19.3 ± 9.9 min ($p < 0.001$) for the medical physicist.

As given in Fig. 5 for re-planned cases based on script-based spheres, mean (standard deviation) values for 1) PTV_6670 V66.7 Gy and CI, 2) PTV_2000 V20Gy and CI, 3) monitor unit ratio and 4) dose ratio were 1) 99.0 % (2.2 %) and 1.31 (0.31), 2) 95.9 % (1.6 %) and 1.05 (0.08), 3) 4.01 (1.39) and 4) 3.24 (0.15). In comparison, on clinical plans these values were 1) 97.3 % (6.6 %) and 1.25 (0.15), 2) 94.6 % (5.0 %) and 1.12 (0.18), 3) 3.64 (1.29) and 4) 3.21 (0.30). No significant differences between plans were measured for any investigated metric (see tabular

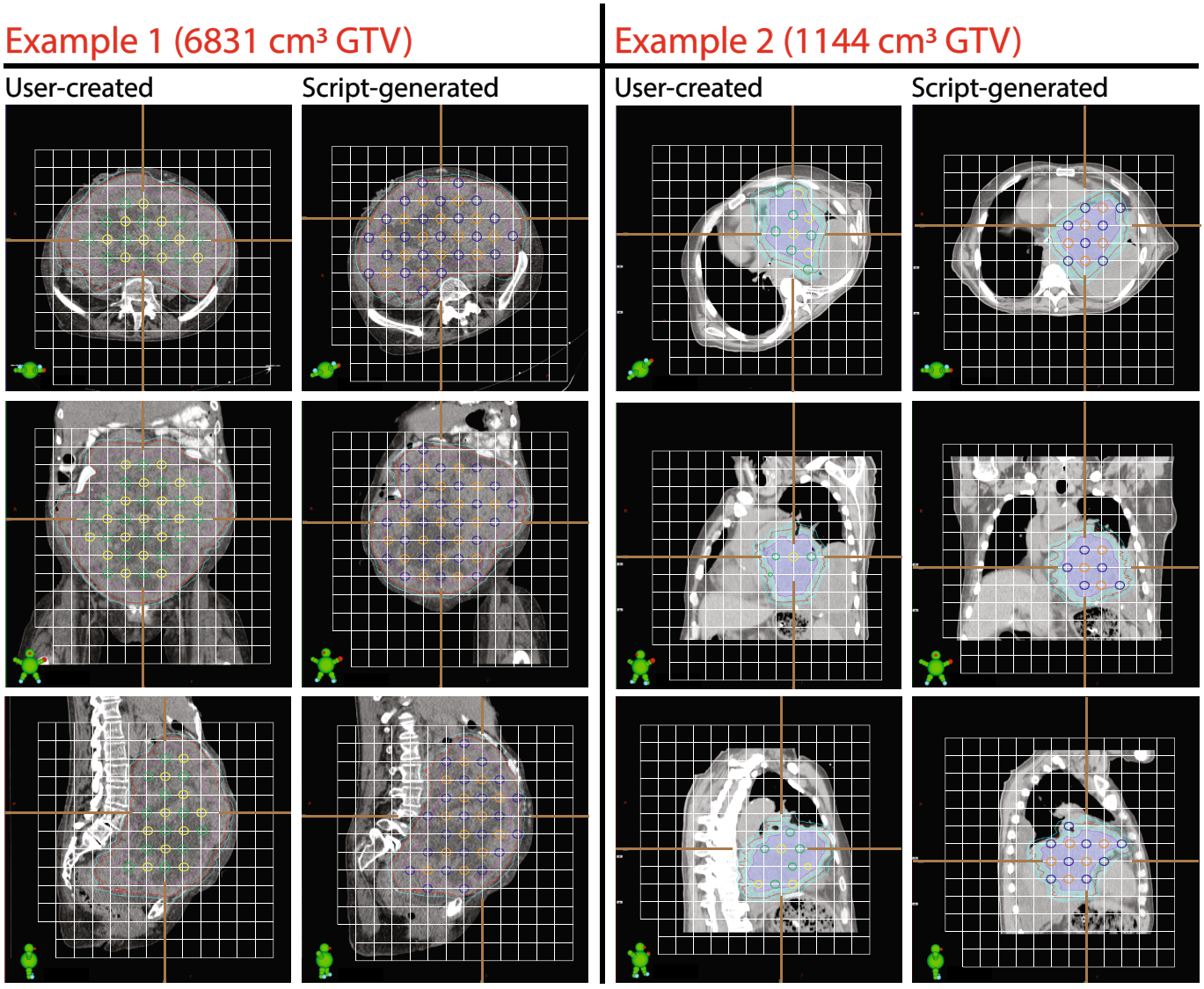

Fig. 3. Two examples of script-based sphere placement in comparison with clinically-used spheres. Images are rotated axially to demonstrate lattice structure relative to patients in each case. In example 1, on the user-created HDS are visibly omitted from several eligible positions and LDS do not extend to the PTV_2000 border. In this example, the script-generated spheres produced a pattern on a grid rotated about the cranial-caudal axis. In example 2, several rule violations are apparent in the HDS on the clinical plan while in contrast no violations are evident on the script-generated spheres. In both examples, HDS are shown in yellow (user-created) and orange (script), and LDS are green (user-created) and blue (script). (For interpretation of the references to colour in this figure legend, the reader is referred to the web version of this article.)

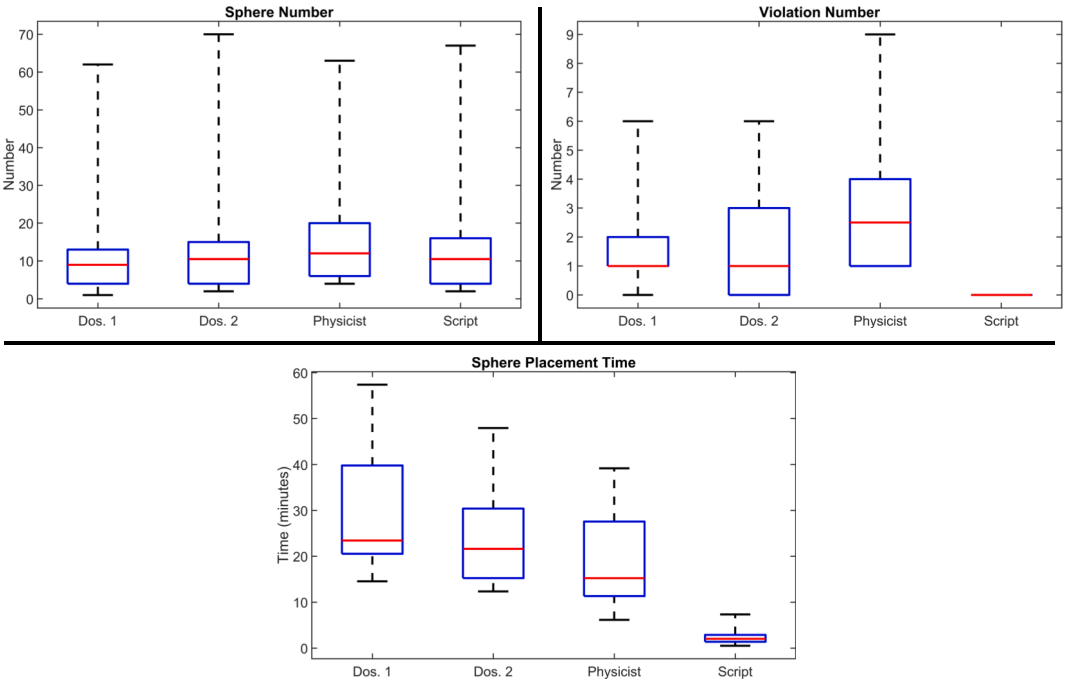

Fig. 4. Box-whisker comparison of sphere number (top left), violation number (top right) and sphere placement time (bottom) between clinicians (including two dosimetrists and physicist) and script. Red denotes median values, blue boxes are inter-quartile ranges, and dashed black lines are entire ranges. Sphere numbers do not include manually-removed spheres for two cases, as discussed in text. (For interpretation of the references to colour in this figure legend, the reader is referred to the web version of this article.)

data in supplementary material). All institutional OAR dose constraints were met on all re-planned cases except two. In one case, PTV_2000 and GTV overlapped the entire bladder and a script-produced sphere partially overlapped bladder. In a second case, PTV_2000 and GTV significantly overlapped heart, and a script-generated sphere overlapped heart. In these cases, constraints were not met (bladder D0.035 cm^3 < 38 Gy and heart D0.03 cm^3 < 38 Gy). These two spheres overlapping OARs were manually removed, and resulting plans then met constraints.

4. Discussion

Several studies – like those by Grams et al., Wu et al, and Borzov et al. – utilize concepts similar to those folded into the presented script in this study [14,15,22]. For example, these studies include minimum distances between high dose vertices and also confine high dose regions within gross tumor. These studies also leverage the expertise of radiation oncologists, medical physicists and dosimetrists to generate a sensible spatial fractionation pattern. While these studies among others are similar in these aspects, these approaches to spatial fractionation differ sufficiently to complicate inter-comparison. For example, in certain studies distances between high doses can be variable, certain studies plan to high dose spheres while others target cylinders, and the size of the high dose vertices can be variable both across approaches and even within certain approaches. With script-based implementation of lattice SBRT, we strive to motivate standardization for better multi-institutional inter-comparison [27].

Script-based placement with tunable parameters can also facilitate efficient and well-controlled evaluation of planning indices for different geometries. For example, SFRT is increasingly being explored and applied in intensity modulated proton therapy where differences between beamlines and planning techniques can result in variable dosimetry in terms of indices like peak-to-valley dose [28–32]. Through script-based vertex placement, recipes can be designed that relate metrics like peak-to-valley dose to vertex spacing and size [33].

The script-based approach significantly decreased time required for sphere placement in comparison to manual sphere placement. While sphere number was not greater using the script in every case, significantly more spheres excluding violations were placed by the script. By virtue of its rule-based approach, no sphere violations were identified with the script. In contrast, at least one violation was identified in every case for the spheres placed by the physicist, which corresponds in most cases to the clinically-used sphere arrangement. While these plans were deemed clinically acceptable in terms of sphere proximity to OARs, these violations can be user-dependent with more experienced planners' better understanding what translates to an acceptable violation. Script-based placement removes dependency on user-experience and ensures an appropriate number of spheres are placed, thus removing a significant obstacle for accessibility to lattice SBRT.

Especially for smaller GTVs – particularly with non-spherical aspect ratios – that accommodate fewer than 10 HDS, manually-placed spheres are prone to rule violations due to tendencies to try to fit additional spheres within the GTV retraction. For four cases, the script was able to only fit three or fewer spheres into the GTV. In certain cases like these, user-placed spheres relaxed sphere spacing rules in effort to include an additional sphere. While these arrangements led to clinically acceptable plans in terms of OAR sparing, in principle these deviations could produce outlying lattice-specific plan indices such peak-to-valley dose ratio (quantified here by the *dose ratio* metric). Ultimately, no data indicates that higher sphere number supports better clinical results, and we purport that ensuring the fidelity of the grid pattern with its associated dose gradients is of greatest importance to supporting the hypotheses underlying lattice SBRT [34].

Our findings indicate that the script reliably preserves the grid structure we previously outlined while also reducing treatment planning time. In all cases except two, re-planning with script-produced spheres yield plans in which clinically-defined dose objectives remained met. For the two cases with unmet constraints, we manually removed two spheres (one per plan) that overlapped OARs, and re-optimized plans then met constraints. Similarly, on several clinical plans we removed spheres after review of dose on a first plan to reduce dose to specific OARs and support safer localization of the HDS. To further expedite treatment planning with script-produced spheres, a modified structure

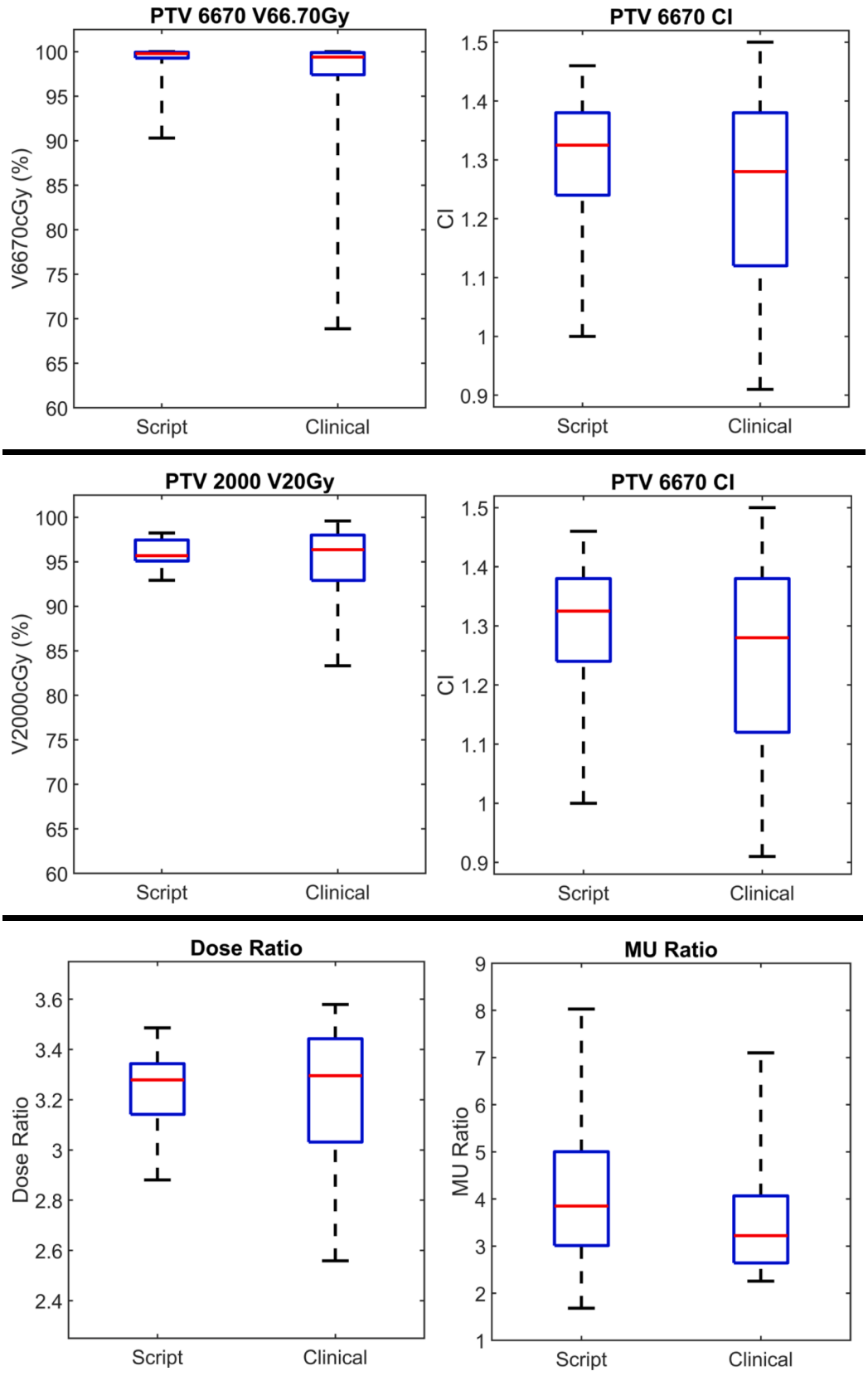

Fig. 5. Box-whisker comparisons of plan quality indices between clinical lattice plans and plans created with script-generated spheres. Red denotes median values, blue boxes correspond to inter-quartile ranges, and dashed black lines indicate total range. (For interpretation of the references to colour in this figure legend, the reader is referred to the web version of this article.)

derived from the PTV that excludes regions of interest (e.g. OARs, bone, regions of re-irradiation, etc.) can be defined as the sphere boundary in a future script iteration.

With this rule-based script, we can readily accommodate adjustments to key parameters. For example, the GTV retraction is a user-tunable parameter which can be adjusted case-by-case per discretionary experience. In a future version of this script, the sphere diameter and grid spacing could also be adjusted to investigate alternative geometries. Given that we often plan these palliative cases urgently, building more sophisticated rules should further expedite treatment planning by producing a sphere arrangement that should not require modification after initial optimization. Most importantly, the script enforces rule-based sphere placement, and so supports standardization of dosimetry which is critically important for meaningfully evaluating treatment response [35].

In this study, we compared automated sphere placement with manual sphere placement for lattice SBRT. We demonstrated that script-based sphere generation significantly decreased planning time and also significantly increased the number of spheres placed that are compliant with protocol rules. We also demonstrated that plan quality as characterized by lattice-specific metrics and institutional OAR constraints remained met in most cases when planning based on script-generated spheres. We envision sharing this tool upon request to enable standardized application of lattice SBRT with other sites and potentially even support multi-institutional studies on lattice SBRT.

CRediT authorship contribution statement

Wesley W. Tucker: Conceptualization, Methodology, Software, Validation, Formal analysis, Investigation, Data curation, Writing – original draft. **Thomas R. Mazur:** Conceptualization, Validation, Writing – original draft. **Matthew C. Schmidt:** Software, Writing – review & editing. **Jessica Hilliard:** Investigation, Data curation. **Shahed Badiyan:** Resources, Writing – review & editing. **Matthew B. Spraker:** Conceptualization, Resources, Writing – review & editing, Supervision. **James A. Kavanaugh:** Conceptualization, Software, Validation, Formal analysis, Investigation, Data curation, Writing – original draft.

Declaration of competing interest

The authors declare that they have no known competing financial interests or personal relationships that could have appeared to influence the work reported in this paper.

Appendix A. Supplementary data

Supplementary data to this article can be found online at https://doi.org/10.1016/j.phro.2024.100549.

References

[1] Mohiuddin M, Fujita M, Regine WF, Megooni AS, Ibbott GS, Ahmed MM. High-dose spatially-fractionated radiation (GRID): a new paradigm in the management of advanced cancers. Int J Radiat Oncol Biol Phys 1999;45:721–7. https://doi.org/10.1016/S0360-3016(99)00170-4.

[2] Iori F, Cappelli A, D'Angelo E, Cozzi S, Ghersi SF, De Felice F, et al. Lattice Radiation Therapy in clinical practice: A systematic review. Clin Transl Radiat Oncol 2023;39:100569. https://doi.org/10.1016/j.ctro.2022.100569.

[3] Yan W, Khan MK, Wu X, Simone CB, Fan J, Gressen E, et al. Spatially fractionated radiation therapy: history, present and the future. Clin Transl Radiat Oncol 2020;20:30–8. https://doi.org/10.1016/j.ctro.2019.10.004.

[4] Marks H. A new approach to the roentgen therapy of cancer with the use of a grid. J Mt Sinai Hosp N Y 1950;17:46–8.

[5] Marks H. Clinical experience with irradiation through a grid. Radiology 1952;58:338–42. https://doi.org/10.1148/58.3.338.

[6] Harris W. Recent clinical experience with the grid in the X-ray treatment of advanced cancer. Radiology 1952;58:343–50. https://doi.org/10.1148/58.3.343.

[7] Freid JR, Lipman A, Jacobson LE. Roentgen therapy through a grid for advanced carcinoma. Am J Roentgenol Radium Ther Nucl Med 1953;70:460–76.

[8] Asur R, Butterworth KT, Penagaricano JA, Prise KM, Griffin RJ. High dose bystander effects in spatially fractionated radiation therapy. Cancer Lett 2015;356:52–7. https://doi.org/10.1016/j.canlet.2013.10.032.

[9] Allibhai Z, Taremi M, Bezjak A, Brade A, Hope AJ, Sun A, et al. The impact of tumor size on outcomes after stereotactic body radiation therapy for medically inoperable early-stage non-small cell lung cancer. Int J Radiat Oncol Biol Phys 2013;87:1064–70. https://doi.org/10.1016/j.ijrobp.2013.08.020.

[10] Neuner G, Mohiuddin MM, Vander Walde N, Goloubeva O, Ha J, Yu CX, et al. High-dose spatially fractionated GRID radiation therapy (SFGRT): A comparison of treatment outcomes with cerrobend vs. MLC SFGRT. Int J Radiat Oncol Biol Phys 2012;82:1642–9. https://doi.org/10.1016/j.ijrobp.2011.01.065.

[11] Peñagarícano JA, Moros EG, Ratanatharathorn V, Yan Y, Corry P. Evaluation of spatially fractionated radiotherapy (GRID) and definitive chemoradiotherapy with curative intent for locally advanced squamous cell carcinoma of the head and neck: initial response rates and toxicity. Int J Radiat Oncol Biol Phys 2010;76:1369–75. https://doi.org/10.1016/j.ijrobp.2009.03.030.

[12] Mohiuddin M, Curtis DL, Grizos WT, Komarnicky L. Palliative treatment of advanced cancer using multiple nonconfluent pencil beam radiation: A pilot study. Cancer 1990;66:114–8. https://doi.org/10.1002/1097-0142(19900701)66:1<114::AID-CNCR2820660121>3.0.CO;2-L.

[13] Huhn JL, Regine WF, Valentino JP, Meigooni AS, Kudrimoti M, Mohiuddin M. Spatially fractionated GRID radiation treatment of advanced neck disease associated with head and neck cancer. Technol Cancer Res Treat 2006;5:607–12. https://doi.org/10.1177/153303460600500608.

[14] Grams MP, Owen D, Park SS, Petersen IA, Haddock MG, Jeans EB, et al. VMAT grid therapy: A widely applicable planning approach. Pract Radiat Oncol 2021;11:e339–47. https://doi.org/10.1016/j.prro.2020.10.007.

[15] Wu X, Perez NC, Zheng Y, Li X, Jiang L, Amendola BE, et al. The technical and clinical implementation of LATTICE radiation therapy (LRT). Radiat Res 2020:194. https://doi.org/10.1667/RADE-20-00066.1.

[16] Pokhrel D, Bernard ME, Mallory R, St Clair W, Kudrimoti M. Conebeam CT-guided 3D MLC-based spatially fractionated radiation therapy for bulky masses. J Appl Clin Med Phys 2022:23. https://doi.org/10.1002/acm2.13608.

[17] Kavanaugh JA, Spraker MB, Duriseti S, Basarabescu F, Price A, Goddu M, et al. LITE SABR M1: planning design and dosimetric endpoints for a phase I trial of lattice SBRT: dosimetric endpoints for Phase I Lattice SBRT trial. Radiother Oncol 2022;167:172–8. https://doi.org/10.1016/j.radonc.2021.12.003.

[18] Jin J-Y, Zhao B, Kaminski JM, Wen N, Huang Y, Vender J, et al. A MLC-based inversely optimized 3D spatially fractionated grid radiotherapy technique. Radiother Oncol 2015;117:483–6. https://doi.org/10.1016/j.radonc.2015.07.047.

[19] Zhang X, Griffin RJ, Galhardo EP, Penagaricano J. Feasibility study of 3D-VMAT-based GRID therapy. 153303382210864 Technol Cancer Res Treat 2022;21. https://doi.org/10.1177/15330338221086420.

[20] Duriseti S, Kavanaugh J, Goddu S, Price A, Knutson N, Reynoso F, et al. Spatially fractionated stereotactic body radiation therapy (Lattice) for large tumors. Adv Radiat Oncol 2021;6:100639. https://doi.org/10.1016/j.adro.2020.100639.

[21] Duriseti S, Kavanaugh JA, Szymanski J, Huang Y, Basarabescu F, Chaudhuri A, et al. LITE SABR M1: A phase I trial of Lattice stereotactic body radiotherapy for large tumors. Radiother Oncol 2022;167:317–22. https://doi.org/10.1016/j.radonc.2021.11.023.

[22] Borzov E, Bar-Deroma R, Lutsyk M. Physical aspects of a spatially fractionated radiotherapy technique for large soft tissue sarcomas. Phys Imaging Radiat Oncol 2022;22:63–6. https://doi.org/10.1016/j.phro.2022.04.010.

[23] Iori F, Botti A, Ciammella P, Cozzi S, Orlandi M, Iori M, et al. How a very large sarcomatoid lung cancer was efficiently managed with lattice radiation therapy: a case report. Ann Palliat Med 2022;11:3555–61. https://doi.org/10.21037/apm-22-246.

[24] Costlow HN, Zhang H, Das IJ. A treatment planning approach to spatially fractionated megavoltage grid therapy for bulky lung cancer. Med Dosim 2014;39:218–26. https://doi.org/10.1016/j.meddos.2014.02.004.

[25] Benedict SH, Yenice KM, Followill D, Galvin JM, Hinson W, Kavanagh B, et al. Stereotactic body radiation therapy: the report of AAPM Task Group 101. Med Phys 2010;37:4078–101. https://doi.org/10.1118/1.3438081.

[26] Timmerman R. A story of hypofractionation and the table on the wall. Int J Radiat Oncol 2022;112:4–21. https://doi.org/10.1016/j.ijrobp.2021.09.027.

[27] Mayr NA, Snider JW, Regine WF, Mohiuddin M, Hippe DS, Peñagarícano J, et al. An international consensus on the design of prospective clinical-translational trials in spatially fractionated radiation therapy. Adv Radiat Oncol 2022;7:100866. https://doi.org/10.1016/j.adro.2021.100866.

[28] Grams MP, Tseung HSWC, Ito S, Zhang Y, Owen D, Park SS, et al. A Dosimetric comparison of lattice, brass, and proton grid therapy treatment plans. Pract Radiat Oncol 2022;12:e442–52. https://doi.org/10.1016/j.prro.2022.03.005.

[29] Henry T, Ureba A, Valdman A, Siegbahn A. Proton grid therapy: a proof-of-concept study. Technol Cancer Res Treat 2017;16:749–57. https://doi.org/10.1177/1533034616681670.

[30] Mohiuddin M, Lynch C, Gao M, Hartsell W. Early clinical results of proton spatially fractionated GRID radiation therapy (SFGRT). Br J Radiol 2020;93:20190572. https://doi.org/10.1259/bjr.20190572.

[31] Gao M, Mohiuddin MM, Hartsell WF, Pankuch M. Spatially fractionated (GRID) radiation therapy using proton pencil beam scanning (PBS): feasibility study and clinical implementation. Med Phys 2018;45:1645–53. https://doi.org/10.1002/mp.12807.

[32] Yang D, Wang W, Hu J, Hu W, Zhang X, Wu X, et al. Feasibility of lattice radiotherapy using proton and carbon-ion pencil beam for sinonasal malignancy. Ann Transl Med 2022;10:467. https://doi.org/10.21037/atm-21-6631.

[33] Zhang W, Lin Y, Wang F, Badkul R, Chen RC, Gao H. Lattice position optimization for LATTICE therapy. Med Phys 2023;50:7359–67. https://doi.org/10.1002/mp.16572.
[34] Rivera JN, Kierski TM, Kasoji SK, Abrantes AS, Dayton PA, Chang SX. Conventional dose rate spatially-fractionated radiation therapy (SFRT) treatment response and its association with dosimetric parameters—A preclinical study in a Fischer 344 rat model. PLoS One 2020;15:e0229053.
[35] Giglioli FR, Garibaldi C, Blanck O, Villaggi E, Russo S, Esposito M, et al. Dosimetric multicenter planning comparison studies for stereotactic body radiation therapy: methodology and future perspectives. Int J Radiat Oncol Biol Phys 2020;106:403–12. https://doi.org/10.1016/j.ijrobp.2019.10.041.